Recovery of Light Oil by Air Injection

Negar Khoshnevis Gargar [*], Alexei A. Mailybaev [†], Dan Marchesin [‡], Hans Bruining [§]

June 24, 2014

Abstract

Nomenclature

A_r	MTO reaction pre-exponential factor, 1/s
α	oleic (o), aqueous (w) and gaseous (g) phase
c_α	heat capacity of phase α (o, w, g), J/(mol·K)
C_m	heat capacity of porous matrix, J/(m^3·K)
n	MTO reaction order with respect to oxygen
P_g	gas pressure, Pa
P_{res}	reservoir pressure, Pa
Q_r	MTO reaction enthalpy per mole of oxygen at reservoir temperature, J/mol
Q_{vh}, Q_{vw}	oil and water vaporization heat at reservoir temperature, J/mol
R	ideal gas constant, J/(mol·K)
s_α	saturations of phase α
s_o^{ini}, s_w^{ini}	initial saturations of oil and water phase in the reservoir
T	temperature, K
T^{ini}	initial reservoir temperature, K
T^{ac}	MTO activation temperature, K
u_α	Darcy velocity of phase α, m/s
u_{gj}	Darcy velocity of component $j = h, \kappa, w, r$ in gas phase, m/s
u_{inj}	Darcy velocity of injected gas, m/s
W_r	MTO reaction rate, mol/(m^3·s)
W_{vh}, W_{vw}	vaporization rate for hydrocarbon and water, mol/(m^3·s)
x, t	spatial coordinate, m, and time, s
Y_h, Y_κ, Y_w, Y_r	gas molar fractions: hydrocarbons, oxygen, steam, remaining components, mol/mol
Y_κ^{inj}	oxygen fraction in injected gas
λ	thermal conductivity of porous medium, W/(m·K)
ν_l, ν_g, ν_w	stoichiometric coefficients in the MTO reaction
ρ_α	molar density of phase α, mol/m^3

[*]Delft University of Technology, Civil Engineering and Geosciences, Stevinweg 1, 2628 CE Delft, The Netherlands. E-mail: N.khoshnevisgargar@tudelft.nl

[†]Instituto Nacional de Matemática Pura e Aplicada (IMPA), Estrada Dona Castorina 110, Rio de Janeiro 22460-320, Brazil. E-mail: alexei@impa.br

[‡]Instituto Nacional de Matemática Pura e Aplicada (IMPA), Estrada Dona Castorina 110, Rio de Janeiro 22460-320, Brazil. E-mail: marchesi@impa.br

[§]Delft University of Technology, Civil Engineering and Geosciences, Stevinweg 1, 2628 CE Delft, The Netherlands. E-mail: J.Bruining@tudelft.nl

Introduction

Air injection leading to in-situ combustion is generally considered applicable to recovery of heavy oils because it causes a significant reduction in oil viscosity. The air injection process usually refers to "high pressure air injection" (HPAI), whereas the term "in-situ combustion" traditionally has been used for heavy oil reservoirs. In this process, the oxygen in the injected air burns the heavier components of the oil, thus generating a heat wave leading to cracking of heavier components and vaporization of lighter components. Air injection has the advantage of ready air availability at any location [52]; however, energy costs of air compression necessary for injection are not negligible. Air injection can also be used to recover light oils by mechanisms such as combustion gas drive, distillation and thermal expansion [16, 18, 22, 54, 49, 23, 5, 2]. This work considers a new combustion mechanism to enhance recovery of light oil by air injection.

It is worth noting that water injection is not an efficient recovery method in low permeability heterogeneous reservoirs due to poor sweep efficiency [55, 10]. There is a large body of literature describing the use of HPAI (high pressure > 100 bars air injection) to recover oil [1, 3, 11, 13, 14, 36, 39, 40, 56, 59]. HPAI was first introduced in 1979 in the Buffalo field [17]. The effectiveness of HPAI depends on many oil recovery mechanisms [15] including sweeping by flue gases, field repressurization by the injected gas, oil swelling, oil viscosity reduction, stripping off light components in the oil by flue gas and thermal effects generated by the oxidation reactions. The displacement efficiency of oil recovery in combustion processes is the initial oil-in-place excluding the amount of fuel consumed in combustion, i.e., the residual oil is produced [45]. However to reduce the high compression costs and to avoid fracturing at shallower depth, our focus will be an alternative to HPAI, i.e., to inject air at medium pressures ($\sim 10 - 90$ bars). The main recovery mechanism that we consider for medium pressures is the interaction between vaporization and combustion of light oil.

The combustion mechanism varies with the type of oil. In summary, we have high temperature oxidation (HTO) [41], in which cracking occurs forming coke, which is subsequently oxidized at high temperatures; low temperature oxidation (LTO), in which the oxygen is adsorbed or incorporated by the hydrocarbon molecules to form alcohols, aldehydes, acids or other oxygenated hydrocarbons [26, 27, 30]; and medium temperature oxidation (MTO) [22, 27, 28], when the oxidation reaction leads to scission of the molecules into small reaction products such as water, CO or CO_2.

The mathematical theory of combustion in porous media is well developed for immobile fuels, see, e.g., [9, 11, 48, 51, 56]. When the fuel is liquid and can also vaporize, the problem becomes more complicated. It was shown in [43] that, in the case of liquid fuel, the combustion wave has a resonant structure similar to that encountered earlier in detonation problems, see [19, 37, 53, 58]. The mathematical theory shows that the recovery is most efficient when such a resonance occurs. In this case at some point in the internal structure (resonant point) of the wave, the Buckley-Leverett characteristic speed is equal to the combustion velocity.

In this paper, we review extensively the model suggested in [44] for air injection in light oil leading to medium temperature oxidation (MTO). The mechanisms operating in MTO have received little attention in the literature [27, 25, 24, 22, 29]. The main purpose of this paper is to elucidate the prevailing mechanisms in MTO. Therefore we developed a simple 1-D model considering light oil recovery through displacement by air at medium pressures and low injection rates and performed both numerical and laboratory experiments to validate the theory. The presence of liquid fuel, which is mobile and can vaporize or condense, is a challenge for modeling the combustion process [23]. The low air injection rate was chosen to mimic the processes in the main reaction zone (away from the injection well) in an oil reservoir. We only consider the one dimensional flow problem, expecting that its solution contributes to understanding the MTO process and determining the displacement efficiency.

The mathematical model is given by a system of multi-phase flow equations with additional

terms describing reaction and vaporization rates, and an energy balance equation. Analytically, the general solution is composed of three types of nonlinear waves, which are a thermal, a combustion and saturation waves [44]. In MTO, all physical processes, reaction, vaporization, condensation and filtration, are active. The name of the wave (MTO) comes from the fact that the maximum temperature is bounded by the liquid boiling temperature and, thus, cannot become very high. One of the main issues investigated in this work is the relative importance of vaporization/condensation/oxidation for light oil recovery in an MTO process.

The detailed mechanism depends on diffusive processes (capillary, molecular diffusion and heat conductivity), oil composition, air injection rate, pressure, presence of water and water saturation. The theory gives the ratio between the oil recovered and the oil burnt, and describes the behavior of oil mixtures (here modeled as two-component mixtures). One of the purposes of our research is to investigate whether we can find experimental evidence for the combustion mechanism described theoretically. We perform and interpret experiments involving air injection in a consolidated porous medium filled with one-component oil (hexadecane) at medium pressures to validate the theory and to find details of the oxidation mechanisms. As we use conditions that are representative further away from the well, we expect to see details relevant in the field that are not visible for experiments operating at high rates and high pressures [7, 29, 22, 40, 27], which are representative in the near well bore region.

The paper is organized as follows. Section 1 describes the physical model and presents governing equations briefly. Section 2 describes analytical solutions of medium temperature oxidation process. Section 3 presents the numerical results for thermal, capillary and mass diffusive processes. In section 4, numerical solutions with several sets of conditions for the two-component oil model are presented. The numerical solutions with several sets of conditions for the oil with different boiling temperatures in the presence of initial water are presented in section 5. Section 6 describes the results of laboratory experiments. We end with some conclusions.

1 Model

We study a three-phase flow problem (gas, oil and water) involving a combustion front when air is injected into thermally isolated porous rock filled with light oil and water. We summarize the reaction process by the following reaction equation:

$$\nu_l(\text{hydrocarbons}) + \text{O}_2 \rightarrow \nu_w\,(\text{H}_2\text{O}) + \nu_g\,(\text{other gaseous products}), \tag{1.1}$$

i.e., one mole of oxygen reacts with ν_l moles of initial (liquid) hydrocarbons generating ν_w moles of water in vapor phase and ν_g moles of gaseous products (CO, CO_2, etc.). This reaction equation is an abbreviated form of a number of intermediate reactions leading to complete scission of hydrocarbon molecules (medium temperature oxidation). We disregard gas-phase reactions, though it is still a matter of debate whether such reactions play a significant role in porous media as annihilation of free radicals at the pore walls drastically reduces the reaction rates [6, 31, 38, 50, 20].

The system is studied for one-dimensional flow in the positive horizontal spatial direction x, allowing for the presence of oil, water and gas. The oil saturation is denoted by s_o, the water saturation by s_w and the gas saturation by $s_g = 1 - s_o - s_w$. In the gaseous phase, we distinguish the molar fraction of hydrocarbon gas Y_h, the molar fraction of steam Y_w and the molar fraction of oxygen Y_κ. The remaining components with molar fraction $Y_r = 1 - Y_\kappa - Y_h - Y_w$ consist of inert components from the injected gas and reaction products. The molar mass balance equations for oil, water and the four gas components are

$$\begin{aligned}
\partial_t(\varphi\rho_o s_o) + \partial_x(\rho_o u_o) &= -\nu_l W_r - W_{vh}, && (1.2)\\
\partial_t(\varphi\rho_w s_w) + \partial_x(\rho_w u_w) &= -W_{vw}, && (1.3)\\
\partial_t(\varphi Y_h\rho_g s_g) + \partial_x(\rho_g u_{gh}) &= W_{vh}, && (1.4)\\
\partial_t(\varphi Y_\kappa\rho_g s_g) + \partial_x(\rho_g u_{g\kappa}) &= -W_r, && (1.5)\\
\partial_t(\varphi Y_w\rho_g s_g) + \partial_x(\rho_g u_{gw}) &= W_{vw} + \nu_w W_r, && (1.6)\\
\partial_t(\varphi Y_r\rho_g s_g) + \partial_x(\rho_g u_{gr}) &= \nu_g W_r, && (1.7)
\end{aligned}$$

Assuming that the temperature of solid rock, oil, water and gas are locally equal, we write the energy balance equation as

$$\frac{\partial}{\partial t}\left((C_m + \varphi c_o\rho_o s_o + \varphi c_w\rho_w s_w + \varphi c_g\rho_g s_g)\,\Delta T\right) + \frac{\partial}{\partial x}\left((c_o\rho_o u_o + c_w\rho_w u_w + c_g\rho_g u_g)\Delta T\right) = \lambda\frac{\partial^2 T}{\partial x^2} + Q_r W_r - Q_{vh}W_{vh} - Q_{vw}W_{vw}, \quad (1.8)$$

where $\Delta T = T - T^{ini}$ is defined with respect to the initial reservoir temperature T^{ini}. In (1.8), C_m, c_o, c_w, c_g are the heat capacities for the rock, the oil phase, water phase and gas phase respectively. We use the ideal gas law to relate the total molar gas density ρ_g to the pressure P_g, and the Darcy velocities with quadratic relative permeability functions for the oil, water and gas phases. The partial pressure of the gaseous hydrocarbon and water in oil-gas and water-gas equilibria are given by combining the Clausius-Clapeyron relation with Raoult's law. We consider the MTO reaction rate as

$$W_r = A_r\varphi\rho_o s_o\left(\frac{P_g Y_\kappa}{P_{atm}}\right)^n \exp\left(-\frac{T^{ac}}{T}\right), \quad (1.9)$$

where A_r is the frequency factor for the oxidation rate of oil. We use $T^{ac} = E_{ac}/R$ to denote the activation temperature for the oxidation reaction, which is related to the activation energy E_{ac}. The vaporization rates W_{vh} and W_{vw} for hydrocarbon and water are assumed to be proportional to the deviation of the mole fraction of the gas component from its equilibrium value.

The initial reservoir conditions for $t = 0$, $0 \le x \le l$ are

$$T = T^{ini}, \quad s_o = s_o^{ini}R(x), \quad s_w = s_w^{ini}R(x), \quad Y_h = Y_h^{eq}, \quad Y_\kappa = 0, \quad Y_w = Y_w^{eq}, \quad P_g = P_{ini}(x), \quad (1.10)$$

where the ramp function $R(x)$ describes continuous change of saturations from zero to their initial reservoir values. This is necessary for numerical purposes. The injection conditions at $x = 0,\ t \ge 0$ are

$$s_o = s_w = Y_h = Y_w = 0, \quad T = T^{ini}, \quad u_g = u_{inj}, \quad Y_\kappa = Y_\kappa^{inj}, \quad (1.11)$$

corresponding to the injection of air at reservoir temperature T^{ini} and constant Darcy velocity u_{inj}. It is assumed that there are neither gaseous hydrocarbons nor water in the injected gas, i.e., $Y_h = Y_w = 0$. For numerical solutions, we need to state the production conditions at $x = l$, $t \ge 0$, which are taken to be

$$\partial_x s_o = \partial_x s_w = \partial_x Y_\kappa = \partial_x Y_w = \partial_x Y_h = \partial_x T = 0, \quad P_g = P_{res}. \quad (1.12)$$

We utilize a fully implicit numerical solution approach based on finite-elements, i.e., we formulate and solve the finite element problem using COMSOL software for the model equations in weak form. The grid size in the simulations is 0.01 m, which is fine enough to capture the multi-scale processes and capable of resolving salient features.

Several modifications of the model described above are also used in this paper, as it will be specified explicitly in each particular case.

A_r	=	4060 1/s	Q_r	=	400 kJ/mol O_2	u^{inj}	=	8.0×10^{-7} m/s
c_g	=	29 J/mol K	Q_{vh}	=	31.8(45)(25) kJ/mol	Y_κ^{inj}	=	0.21
C_m	=	2 MJ/m ^{3}K	R	=	8.314 J/mol K	ν_g	=	0.63 (0.648) (0.625) [mol/mol]
c_o	=	224 J/mol K	s_{or}	=	0.1	ν_l	=	0.09 (0.054) (0.125) [mol/mol]
c_w	=	75 J/mol K	n	=	1	ν_w	=	0.72 (0.7) (0.75) [mol/mol]
D_g	=	10^{-9} m^2/ s	T^{ac}	=	7066 (10050) K	ρ_w	=	55000 mol/m^3
k	=	10^{-10} [m^2]	T^{ini}	=	300 K	ρ_o	=	6826 (4411) (8694) mol/m^3
P_{res}	=	10^6Pa	T^{nh}	=	371 (489) (309) K	φ	=	0.3
Q_{vw}	=	40 kJ/mol	T^{nw}	=	373 K	λ	=	3 W/m K

Table 1: Values of reservoir parameters for heptane (dodecane) (pentane) as effective oil pseudo-component.

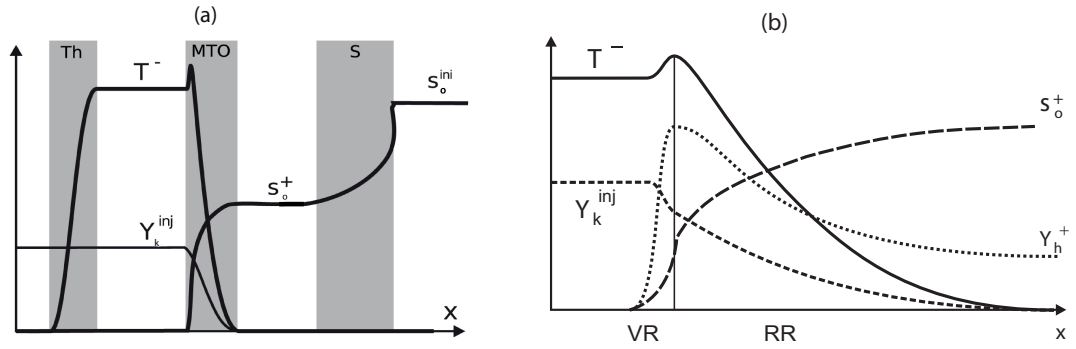

Figure 1: (a) Wave sequence solutions of the thermal (Th), MTO and saturation (S) waves for the combustion of light oil [44]. Indicated are the schematic distributions of the temperature T, oleic saturation s_o and oxygen fraction Y_κ. Superscripts (-) and (+) represent the upstream and downstream side of the MTO wave respectively. The x-axis corresponds to T^{ini} for temperature and to zero for other variables. (b) Schematic graphs of the MTO wave profile. The thin vaporization region (VR) is dominated by vaporization and the much wider reaction region (RR) is dominated by the MTO reaction with slow condensation. The VR is much thinner than the RR, because it is assumed that vaporization is much faster than the reaction.

2 Structure of analytical solution

Here we briefly describe the analytical solution obtained in [44] for a simplified model, where the water phase and thermal diffusion were neglected. The solution corresponds to the long time behavior and consists of a sequence of moving waves separated by constant states. In Fig. 1a the solution is shown as a sequence of three waves, viz., a thermal, an MTO, and a saturation wave. Due to the high heat capacity of the rock, the thermal wave is the slowest. The constant state at the upstream side of the thermal wave is determined by the injection boundary conditions. The temperature in the thermal wave changes from a low value $T = T^{ini}$ upstream to some high value T^- downstream.

The MTO region contains the most interesting traveling wave, which has a constant speed v (Fig. 1b). In this region, all the dependent variables T, s_o, u, Y_h, Y_κ can be expressed in terms of a single traveling coordinate $\xi = x - vt$, *i.e.*, in a frame of reference moving with speed v. Reference [44] uses the traveling wave solution to relate quantities at the upstream side to those at the downstream side, and to obtain the wave speed v. The region upstream of the MTO wave contains injected gas with an oxygen fraction $Y_\kappa^{inj} > 0$ and no gaseous hydrocarbon, $Y_h = 0$. The reaction rate W_r vanishes both at the upstream and downstream side of the MTO region, which leads to the condition $s_o = 0$, (no oil) upstream, and $Y_\kappa = 0$, (no oxygen) downstream. Downstream of the MTO wave there is liquid hydrocarbon with a saturation $s_o^+ > 0$ and a temperature $T = T^{ini}$; here

the equilibrium condition $W_{vh} = 0$ requires $Y_h = Y_h^{eq}(T^{ini})$.

The mathematical analysis of the MTO region is simplified in an essential way by the reasonable physical assumption that the vaporization rate is much higher than the reaction rate. Under this assumption the MTO region is divided into a vaporization region (VR) and a reaction region (RR), see Fig. 1b. The VR is very thin due to high vaporization rate. Here the fraction of gaseous fuel rises from $Y_h = 0$ in the injected gas to the equilibrium value $Y_h = Y_h^{eq}(T)$ at the downstream end of the VR. Since this region is very thin and the reaction rate is not large at the prevailing low fuel concentration, the oxygen consumption in the VR is negligible. In the RR, most of the MTO reaction occurs. Moreover gaseous fuel condenses due to temperature decrease downstream in the direction of gas flow. Along the RR, the equilibrium condition $Y_h = Y_h^{eq}(T)$ holds approximately. The surprising feature of MTO is that the thin VR is located upstream of the RR.

Finally, the saturation wave travels downstream of the MTO wave, see Fig. 1a, where the temperature is constant and equal to $T = T^{ini}$. Therefore, we have thermodynamic equilibrium between liquid and vaporized hydrocarbon, i.e., $Y_h = Y_h^{eq}(T^{ini})$, and there is no net vaporization or condensation. The injected oxygen has been consumed completely in the MTO region. Therefore, we have $Y_\kappa = 0$ downstream of the MTO region, where no reaction occurs. The saturation region sustains a Buckley-Leverett solution, which is obtained using the standard procedure involving the Welge tangent construction [57]. Briefly, from upstream to downstream, the Buckley-Leverett solution consists of a rarefaction, a shock and a constant state with oil saturation s_o^{ini}, as its initial value.

3 Air injection into a porous medium with one-component oil and gas including capillary, thermal and mass diffusion

In this section, we review the results of numerical simulations with COMSOL for a two-phase (oil and gas) model which was extended to account for the capillary effects, as well as gas and thermal diffusion. We consider reservoir parameters values given in Tab. 1 corresponding to heptane (C_7H_{16}) as a fuel. Parameters of the MTO reaction rate vary considerably depending on specific conditions. The availability of reaction rate data is limited. In Tab. 1 we present the MTO rate parameters compatible with experimental results obtained in [21]. In our solutions, the wave speed and limiting states are fortunately weakly dependent on the elusive kinetic parameters.

As shown in Fig. 2 the numerical solution exhibits two regions (thermal and MTO) in the same way as the analytical solution. The saturation region has moved out of sight to the right. The analytical and numerical solution look similar, in spite of the presence of diffusion terms in the numerical solution. For the parameters used by us, the thermal wave is the slowest wave. Therefore, the thermal wave travels in the region of the reservoir from which the liquid and gaseous hydrocarbons were already displaced, i.e., $s_l = 0$. Also, $Y_h = 0$, as the injected gas contains no gaseous hydrocarbons. Therefore, the liquid fractional flow function f_l, the reaction rate w_r and the evaporation rate w_v are all zero. Since there is no reaction in the upstream part of the MTO wave, the oxygen fraction $Y_o = Y_o^{inj}$ is constant. The temperature in the thermal wave changes from the injection value $T = T^{ini}$ upstream to some value T^- in the plateau. The gradual increase is due to the non-zero value of the thermal conductivity. The Darcy velocity upstream of the thermal wave is the injection Darcy velocity $u = u_{inj}$. The MTO region contains the most interesting waves in our solution, viz., evaporation and combustion. The saturation region travels downstream of the MTO wave. In this region, the temperature is equal to the initial temperature $T = T^{ini}$. Downstream of the MTO region there is liquid-gas equilibrium $Y_h = Y_h^{eq}(0)$, and there is neither vaporization nor condensation. The oxygen has been consumed completely in the MTO region. No reaction occurs downstream of the MTO region as the oxygen mole fraction is zero ($Y_o = 0$), see (1.9) and no reaction occurs upstream of the MTO region due to lack of fuel. Since the volume of each phase

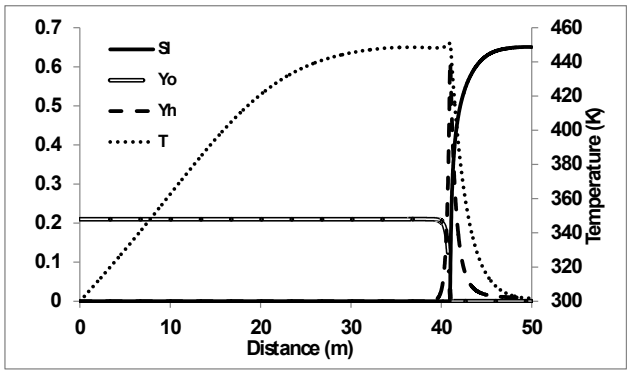

Figure 2: Wave sequence solution with the thermal and MTO regions obtained by numerical simulations. Indicated are the distributions of the temperature T, liquid saturation s_l, oxygen mole fraction Y_o and gaseous hydrocarbon mole fraction Y_h at $t = 4 \times 10^7 sec$ in base case related to Table 1. Note near $x = 40$m the abrupt decay of the oxygen concentration, the narrow peak of the Y_h concentration, and the rapid decay in temperature. Consequently the reaction region (RR) and the vaporization region (VR) are also narrow and partly overlapping.

remains constant, the total Darcy velocity is also constant in regions of constant temperature.

The width of the reaction region (RR) evaluated by the decline of the oxygen concentration is of the order of one meter in the diffusive simulation shown in Fig. 2, while the width in the diffusionless analytical solution is of the order of millimeters. This discrepancy is due to both physical (molecular, capillary and thermal diffusion) and numerical diffusion, all present in the simulation. The vaporization rate is made very fast by the application of a high transfer function in the numerical computations or by using thermodynamic equilibrium in the analytical computations. In the RR, the wave profile is characterized by steep changes in all variables at higher temperatures, followed by slower variations at lower temperatures downstream (see Fig. 1). Note also that the temperature T attains a maximum at a peak that determines the resonance state. At this state the heat consuming vaporization at the VR is replaced by the heat providing combustion process in the reaction region (RR). As shown in Fig. 1, the oxygen mole fraction Y_o, the gaseous hydrocarbon mole fraction Y_h and temperature T change more steeply in the RR wave than the corresponding profiles in Fig. 2. Note that T^- is equal to $T^{ini} + 0.85(T^b - T^{ini})$ in Fig. 2, which means that the temperature at the upstream part of the MTO region is 177^oC. This value is between the boiling point T_b and the temperature predicted analytically with a simplified model. Indeed, the temperature upstream of the MTO region increases to become closer to T^b by taking into account the diffusive processes to the model, as was already conjectured in [44]. The liquid saturation downstream of the MTO region, s_l^+ in Fig. 2, is about 0.65 as opposed to 0.56 in the analytical solution.

4 Air injection into a porous medium with two-component oil and gas

In this section, we review the results of numerical simulations for a two-phase (oil and gas) model, where two different oil pseudo-components are distinguished. These two components correspond to light and medium oil fractions. The molar fractions of these components in oil phase are denoted by ψ_l (light) and ψ_m (medium). We consider the reservoir parameters given in Table 1 corresponding to heptane (C_7H_{16}) and decane ($C_{10}H_{22}$) as light (volatile) and medium (non-volatile) oil fractions.

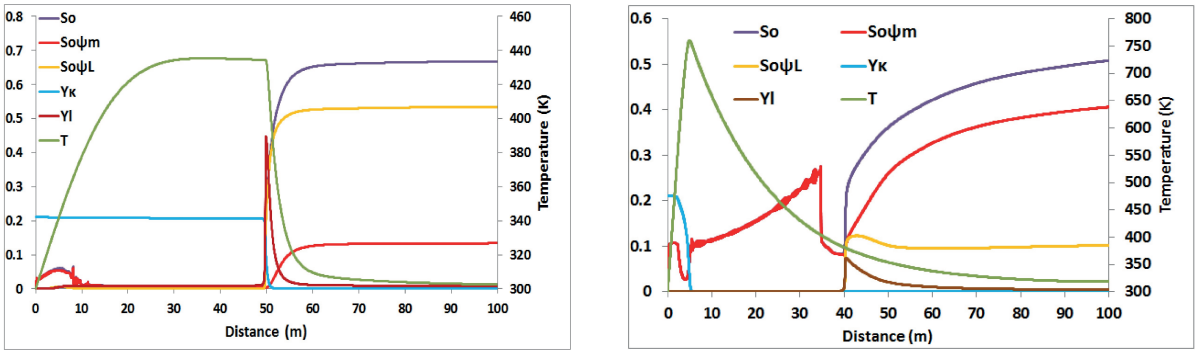

Figure 3: Simulation for an initial medium component fraction of (a) $\psi_m^{ini} = 0.2$ and (b) $\psi_m^{ini} = 0.8$. Wave sequence solution with the thermal and MTO regions. Indicated are the distributions of the temperature T, oleic saturation s_o, oxygen mole fraction Y_κ, gaseous hydrocarbon mole fraction Y_l, light oil concentration $s_o\psi_l$ and medium oil concentration $s_o\psi_m$ at (a) $t = 9.7 \times 10^7 sec$ and (b)$t = 2.1 \times 10^8 sec$.

4.1 Effect of the light (volatile) component fraction

As shown in Fig. 3 (left), the numerical solution exhibits a thermal and an MTO region in the same way as did the analytical solution for the one component system in Fig. 1. In this case the initial volume fraction of the volatile component (C_7H_{16}) is 0.8 in the oil mixture. The saturation region has moved out of sight to the right. For the parameter values used by us, the thermal wave is the slowest wave (it lies between 0 and 25 m in Fig. 3(left)). Therefore, the thermal wave travels in the region of the reservoir from which the light liquid and gaseous hydrocarbons were displaced, i.e., $s_o\psi_l = Y_l = 0$; however small amounts of medium oil remain behind (between $0 - 10m$), upstream of the MTO wave. The reaction rates W_{rl}, W_{rm} and the vaporization rate W_v are all zero or very small in the thermal wave region. Since there is no reaction in the upstream part of the MTO wave, the oxygen fraction $Y_\kappa = Y_\kappa^{inj}$ is constant. The temperature in the thermal wave changes from the injection value $T = T^{ini}$ upstream to some value T^- in the plateau. The Darcy velocity upstream the thermal wave is the injection Darcy velocity $u = u_{inj}$ and it increases downstream due to thermal expansion of gas.

The MTO region contains the vaporization/combustion wave, see Fig. 3 (left). Downstream of the MTO region, the temperature is equal to the initial temperature $T = T^{ini}$. This implies liquid-gas equilibrium $Y_l = Y_l^{eq}(T^{ini})$, and there are neither net vaporization nor condensation. No reaction occurs downstream of the MTO region as the oxygen has been consumed completely in the MTO region ($Y_\kappa = 0$).

In summary when the volatile component represents a large fraction of the oil (in our case $\psi_l^{ini} = 0.8$), vaporization/condensation determines the effectiveness of the combustion process for oil recovery. This effectiveness is more pronounced at lower boiling points. As shown in Fig. 3(left), vaporization of the light component (heptane) occurs upstream of the region of the reaction (of light and medium oil) in the MTO wave (around $50m$ in Fig. 3(left)). Most of the vaporized light component condenses further downstream as the temperature drops down. This fact emphasizes the effectiveness of vaporization/condensation in the displacement of the oil mixture (note the increase of the light component $s_o\psi_l$ as compared to the medium component $s_o\psi_m$ in the upstream side of the MTO wave in Fig. 3). However not all of the non-volatile oil is displaced by the volatile oil, but small amounts remain behind the MTO wave (between $0 - 10m$) because the MTO wave is not initially strong enough to displace the medium oil. This initialization effect causes a slow decrease in the oxygen profile in the first ten meters. The decrease is not visible in Fig. 3 (left) because of the small amounts of fuel and low temperature in that region.

As shown in Fig. 3, the temperature profile is bounded by the boiling temperature ($T^{bl} = 478.5K$) of the volatile fraction at elevated pressure. The oleic saturation downstream of the MTO region is about 0.67, and from this point, the flow continues with a constant state. The Buckley-Leverett profile may follow further downstream, and this profile passed the right end at the time of Fig. 3(left).

4.2 Effect of the medium (non-volatile) component fraction

The two-component system in which one component evaporates and condenses at low or moderate temperatures shows pronounced enhancement of the combustion process effectiveness. Let us study the relative importance of vaporization and combustion in the medium pressure air injection process with different concentrations of the light component. In the base case with medium component volume fraction $\psi_m^{ini} = 0.2$, shown in Fig. 3(left), vaporization occurs upstream of the MTO wave. Single-component studies [44] showed that the combustion front moves considerably faster when vaporization/condensation occurs. In the two-component system $\psi_m^{ini} = 0.2$ shown in Fig. 3(left), the enhancement of oil recovery by distillation is confirmed.

When we increase the medium component fraction to ($\psi_m^{ini} = 0.6$), the general appearance of the solution is preserved. The vaporization region is located upstream of the reaction one. At the upstream side of the MTO region, hydrocarbon evaporates, whereas it condenses at the downstream side.

In Fig. 3(right), the fraction of the medium component in the initial oil was increased to 0.8. As one can see comparing with Fig. 3(left), the general appearance of the waves is not preserved. The oil acts more like immobile fuel in the HTO process [42], though it moves slowly through the domain. Vaporization of the light component occurs downstream of the reaction zone (see the profile of Y_l that starts at $x = 40m$), so that the vaporization is not effective for oil recovery anymore. As shown in Fig. 3(right), most of the light component is swept away by vaporization, while the medium fraction remains behind and reacts with the oxygen in the injected air (at $x = 5m$). The two minima in oil saturation s_o in Fig. 3(right) (at $x = 5m$ and $x = 36m$) are related to combustion and vaporization; we have no correspondence to Fig. 1. In this case, reaction of a large amount of left-behind medium component with oxygen leads to a steep increase in temperature to almost $600°C$ before the latter decreases to its initial value T^{ini} downstream of the condensation region. Since there is no light component in the reaction zone, the temperature is not bounded by the boiling point of the light component. The gaseous hydrocarbon fraction Y_l increases steeply (at $x = 40m$ in Fig. 3(right)) and then condenses gradually downstream to the equilibrium value at the initial temperature. The slow condensation of hydrocarbon from the gas leads to increase in the light oil profile in Fig. 3(right). Note that the behavior near the vaporization region leads to a large oscillation (a large drop followed by an increase downstream) in non-volatile oil component $s_o\psi_m$. The described process has much common with the HTO description in [41, 42]. However there are differences like oscillations in the saturation profile.

We conclude that the MTO wave structure depends drastically on the initial oil composition. When the light component fraction is sufficiently large, the vaporization occurs in the upstream side, leading to effective temperature control and high recovery rate, Fig. 3 (left). On the contrary, when light oil fraction is low, vaporization region moves to the downstream side of the combustion zone, Fig. 3(right). This leads to very high temperatures and slow recovery rate. We should note, however, that our two-component model of MTO is not valid for such high temperatures, because cracking and vaporization of the medium component becomes a relevant part of the process [41, 42]. Thus, our model is only capable to predict a qualitative change of the combustion regime, while a specific profile in the case of Fig. 3(right) must be confirmed using a different model; the latter is a topic for a future research.

5 Air injection into a porous medium with one-component oil, gas and water

In this section, the numerical results are presented for the full three-phase (gas, water and oil) model with a single pseudo-component oil. The effects of the oil boiling point (heptane, dodecane and pentane) and of initial water saturation on oil recovery by the MTO wave are studied.

5.1 Medium boiling point oil

Figure 4 shows the numerical results for the combustion of heptane with the initial saturation $s_o^{ini} = 0.7$, when part of the water is initially present in the reservoir with $s_w^{ini} = 0.2$ and another part is generated by the reaction. The solution consists of a thermal wave, a water vaporization front, an MTO wave (reaction, vaporization and condensation of oil at the steam condensation front), and a saturation wave. As shown in Fig. 4 (left), the temperature in the slowest thermal wave increases from $T^{ini} = 300$K upstream to the value $T^- = 410$ K downstream. At $x = 16$ m, there is a front where the steam is vaporized, and the porous medium contains water at almost initial saturation $s_w \approx 0.2$ downstream.

The MTO wave starts at $x = 41m$. Hydrocarbon vaporization and MTO occur in a very thin region in the upstream part of the MTO wave. All oxygen (blue curve) is consumed in this region. Further downstream at $x > 41$ m, the steam condenses abruptly generating a water jump. The gaseous hydrocarbon Y_h and steam Y_w condense at the same location, which means that the steam condensation front (SCF) moves with the same speed as the MTO wave. All oil is swept by the MTO wave, so that $s_o = 0$ and $Y_h = 0$ upstream of the MTO wave. No oxygen is left in the downstream side, $Y_\kappa = 0$. Overall mass balance considerations show that most of the steam originates from the initial water in the reservoir, while only about 10% comes from the combustion reaction.

Finally, the saturation wave travels downstream of the MTO wave at $x = 42.7$ m in Fig. 4 (left). In this wave, the temperature is low. Therefore, we have thermodynamic equilibrium between vapor and liquid heptane and between steam and water, i.e., $Y_h = Y_h^{eq}(T^{ini})$ and $Y_w = Y_w^{eq}(T^{ini})$, and there is almost no net vaporization or condensation in the saturation wave. The water saturation drops down from $s_w = 0.5$ to the initial value $s_w = 0.2$, while oil saturation jumps from $s_o = 0.2$ to 0.4 followed by a slow increase till $s_o = 0.45$. This wave represents the slowest saturation wave. Recall that several saturation waves typically appear for three-phase flow [4, 46] and the faster saturation waves were only observed at earlier times and moved away to the right.

The behavior just described reveals a complex mechanism, where the coupling of MTO with vaporization/condensation of both steam and oil lead to enhanced recovery. This mechanism has multiple components. The steam vaporization upstream of the MTO wave with condensation downstream increases the gas drive and creates a water bank of high saturation (up to $s_w = 0.5$) in the interval $41 \le x \le 42.7$ m, see Fig. 4 (left). The two-stage oil bank is created first by the oil vaporization/condensation mechanism ($s_o = 0.2$ in $41 \le x \le 42.7$ m), followed by the saturation shock wave leading to the plateau with $s_o = 0.45$. Figure 4 (left) shows that for medium boiling point oil (heptane) the MTO wave and the SCF merge into a single wave; the first evidence for this mechanism was found by Bruining and Marchesin [12]. At the same time, the saturation wave is slightly faster than the MTO wave. So the water and oil banks get wider in time.

When the numerical results for heptane in the absence of initial water (Fig. 2) are compared with the numerical results for a mixture of water and heptane (Fig. 4 (left)), one can observe that the presence of initial water has a positive effect on the recovery of light oil. Oil and water banks are built up, which does not happen in the absence of initial water. In the presence of water, the MTO wave speed is slightly higher, while maximum temperatures are almost the same in both cases.

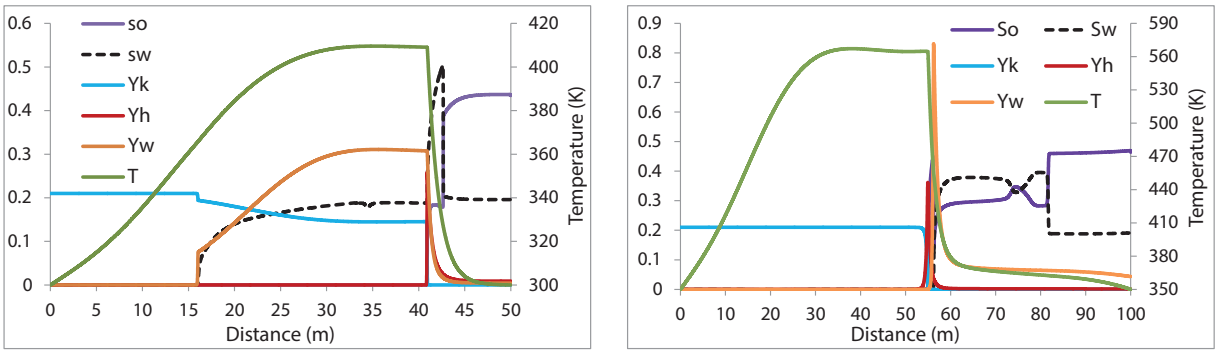

Figure 4: Air injection into (a) heptane/water mixture and (b) dodecane/water mixture with initial saturations $s_o^{ini} = 0.7$ and $s_w^{ini} = 0.2$. Indicated are the distributions of the water saturation s_w, oil saturation s_o, temperature T, oxygen mole fraction Y_κ, steam mole fraction Y_w, and gaseous hydrocarbon mole fraction Y_h at (a) $t = 3.1 \times 10^7 sec$ and (b) $t = 5.5 \times 10^7 sec$.

5.2 High boiling point oil

Let us now consider the effect of water in the air injection process for the recovery of a high boiling temperature oil (dodecane), i.e., when the oil boiling temperature is much higher than that of water. For such oil, we need higher initial temperatures for ignition of the MTO process, and we use $T^{ini} = 350$K. Figure 4 (right) shows the numerical results for the combustion of dodecane when water is initially present in the reservoir with saturation $s_w^{ini} = 0.2$. The initial oil saturation is $s_o^{ini} = 0.7$. The solution consists of a thermal wave, an MTO wave and a saturation wave. As shown in Fig. 4 (right), the (green) temperature in the thermal wave increases from T^{ini} upstream to the value $T^- = 560$ K further downstream.

As one observes by comparing Figs. 4(left) and 4 (right), the position of the steam region relative to the MTO wave changes. Both vaporization and condensation of steam occur downstream of the MTO wave for high boiling point oil. The reason is that the high boiling temperature volatile oil finds it difficult to vaporize and therefore the oil combustion and vaporization/condensation remains upstream. The oxygen mole fraction is constant ($Y_\kappa = Y_\kappa^{ini}$) upstream of the MTO wave, and decreases steeply to zero in the MTO wave at 55m due to the reaction. No oil exists upstream of the MTO wave ($x < 55$m in Fig. 4 (right)). The first increase of oil saturation s_o (purple curve) at $55m$ is a result of mechanisms involving the MTO wave. This includes the reaction as well as condensation of the oil, which was vaporized upstream and carried to colder region in gas form. The oil saturation increases to the maximum $s_o = 0.45$ at $x = 56$m, where it drops down to $s_o = 0.14$ at the boundary of the water region. Finally, there is a saturation wave in the region $70 \leq x \leq 81$ m where the oil saturation rises to $s_o = 0.45$, while water saturation drops to $s_w \approx 0.2$.

As opposed to the case of medium boiling point oil, in which oil and water condensation occur at the same location with the formation of an oil bank, in the case oil with a high boiling point, oil condensation occurs at the location where water evaporates, and water condenses further downstream of the MTO wave. This leads to a negligible effect of water on the oil recovery, resulting in low ($s_o = 0.3$) oil saturation ahead of the MTO wave. Recovery is improved due to the presence of the saturation wave downstream. Unlike the case of Fig. 4 (left), for higher boiling point oil, no steam and water remain behind the MTO wave.

5.3 Efficiency of the steam region and MTO wave

The amount of oil recovered relative to the amount of initial oil in place versus time is shown in Fig. 6 for heptane, dodecane and pentane. Figure 6a shows the striking universality of the recovery curves for heptane in a wide range of initial water and oil saturation. One can see that the curves

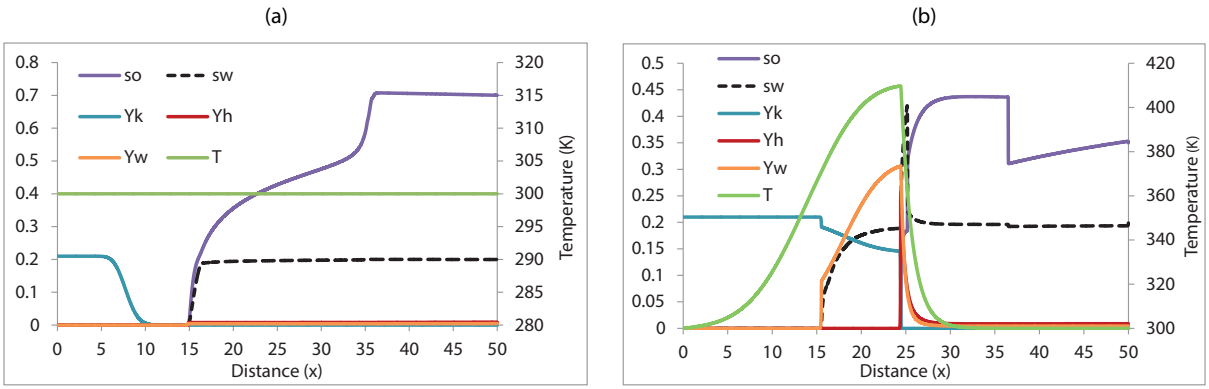

Figure 5: Air injection into a heptane/water mixture with initial saturations $s_o^{ini} = 0.7$ and $s_w^{ini} = 0.2$. Indicated are the distributions of the water saturation s_w, oil saturation s_o, temperature T, oxygen mole fraction Y_κ, steam mole fraction Y_w, and gaseous hydrocarbon mole fraction Y_h at (a) $t = 3 \times 10^6 sec$ (35 days) and (b) $t = 1.6 \times 10^7 sec$ (185 days).

are almost identical to each other. The same figure shows that neglecting water condensation and vaporization in the MTO process (dashed curve) leads to underestimating the recovery, which is enhanced by the steam region. One can clearly distinguish three stages of the recovery history in Fig. 6a, which are characterized by approximately constant recovery rates (slopes). These three stages are the steepest initial part ($0 - 50$ days), the intermediate part with lower recovery rate ($50 - 240$ days) and the final part with a higher recovery rate (> 240 days).

The reservoir states corresponding to the first and second stages are presented in Fig. 5, while the third stage is described in Fig. 4. One can see that the initial recovery (Fig. 5a) is a simple gas displacement in three-phase flow with almost no thermal effects due to reaction ($T \approx T^{ini}$). The recovery mechanism is based on the saturation wave (at 35m in Fig. 5a), which reaches the right end (production side) in about $t = 50$ days. At about the same time, the temperatures increases, leading to the formation of the MTO wave, Fig. 5b. Formation of this MTO wave triggers a secondary saturation wave with a higher speed and lower downstream oil saturation (at 36m in Fig. 5b). This wave is responsible for the small recovery rate in the second stage ($50 - 240$ days in Fig. 6a) due to a lower downstream oil saturation, and it reaches the right end in about $t = 240$ days. The rest of the recovery process is governed by the MTO wave with oil and water banks as described in section 5.1. Note that the last two stages of the recovery are based essentially on the MTO process leading to elevated temperatures. This is why the steam vaporization/condensation plays an important role for improving the recovery rate for $t > 50$ days; compare with the dashed line in Fig. 6a when steam condensation is neglected in the model.

Figure 6b shows the relative recovery curves for dodecane and pentane. The case of pentane is similar to that of heptane (low boiling point) in Fig. 6a. However, we have a different situation for dodecane (high boiling point), where the steam region moves downstream of the MTO wave (Fig. 4 (right)). Several stages can be recognized in this process too. Though, in this case, high initial water saturations lead to considerable decline in oil recovery (green curve in Fig. 6b).

6 Laboratory Experiments

The experimental apparatus is a high pressure ramped-temperature oxidation reactor consisting of a combustion tube (a stainless steel reactor with an internal diameter of 5 cm and a length of 23 cm) equipped with heating devices and equipment for gas injection, sampling and analysis. This setup can be operated at either a predefined heating rate schedule or at a fixed temperature, medium pressure and low air injection rate. The reactor temperature is determined by four thermocouples

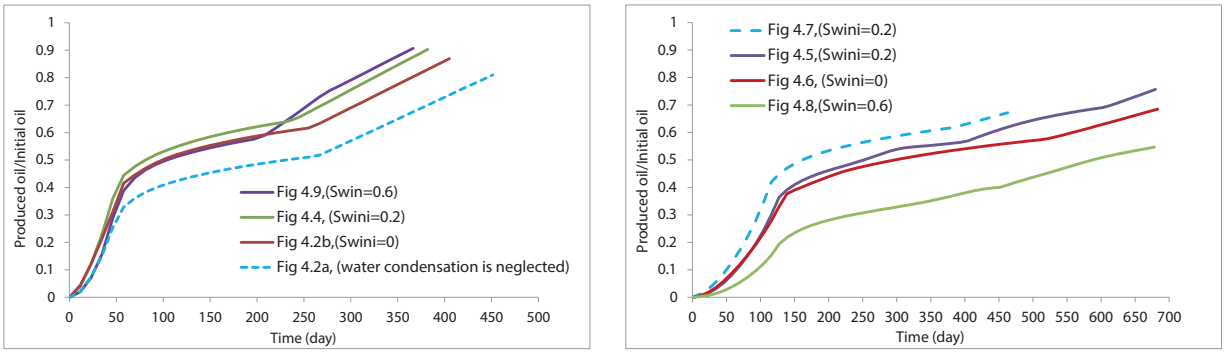

Figure 6: The recovery fraction of oil versus time for (a) heptane and (b) dodecane (solid lines) and pentane (dashed line) obtained by numerical simulations for different initial water saturations s_w^{ini}.

inserted along axis of the sandstone core, from TC-1 at the top to TC-4 at the bottom. Heat is provided by a cylindrical electrical heater enclosing the tube. The complete setup is insulated by thermal ceramic super-wool to minimize heat losses.

A vertically-positioned sandstone core in the high pressure stainless steel reactor is first evacuated and then is entirely saturated with the model oil (n-hexadecane), which was preheated to a desired temperature through a given heating schedule. One of the main favorable features of this type of test is being able to perform all experiments with Bentheimer consolidated sandstone cores, which are rather homogenous. This is opposed to most experiments reported in the literature, generally performed with crushed core or sand, which can alter the original permeability and porosity. The air is injected from the top, controlled by a mass flow meter; oil and exhaust gases are produced at the reactor bottom. The produced gas is analyzed by a gas chromatograph (GC). Liquids from the reactor are collected and analyzed to determine the produced oil viscosity and density. The heating schedule is defined as 10°C/10min, while the injected gas starts to flow through the reactor at a defined rate. The same heating schedule is used for all the experiments.

6.1 Experimental results

For the interpretation of experimental results, we propose the following overall oxidation reaction formula for alkane fuel (hexadecane in our experiments):

$$zC_nH_{2n+2} + qC_nH_{2n+2}O_2 + \frac{1}{\mathcal{R}}O_2 + N_2 \rightarrow \tag{6.1}$$

$$\hat{z}C_nH_{2n+2} + \hat{q}C_nH_{2n+2}O_2 + sH_2O + pCO_2 + vCO + fO_2 + N_2,$$

where the nitrogen/oxygen molar ratio in the injected air is denoted by $\mathcal{R}$, which is equal to 3.7. This model reaction describes sorption of oxygen or formation of oxygenated hydrocarbon when $\hat{q} > q$ and desorption or release of oxygen when $\hat{q} < q$. When $z + q > \hat{q} + \hat{z}$, it also describes full oxidation for a part of hydrocarbon molecules. Hydrogen concentration was not measured in the produced gas, which is a restriction for our GC setup. In the first experiment (Exp. 1), air was injected into the reactor, which was previously saturated completely with hexadecane as the model oil. The reactor was heated from room temperature to $400°C$ at a heating rate of $10°C/10min$. Figure 7 (left) shows the temperature and the produced gas composition histories. The gentle increase up to $150°C$ is due to heating interruption in the experiment because of problems with the back pressure valve, which were resolved after 150 minutes, recovering the initial heating rate.

Deviations of the temperatures along the tube (i.e., in different thermocouples) occur at temperatures above $200°C$, which is an indication of heat release due to sorption of oxygen in the

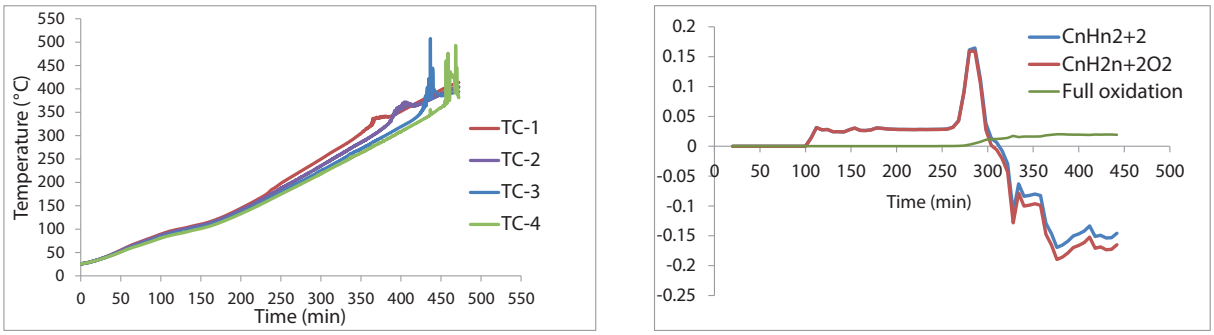

Figure 7: (a) temperature measurement history for air injection. (b)Reaction rates based on the reaction model. The blue curve shows the stoichiometric coefficient history $z - \hat{z}$ describing the reaction rate of hexadecane. The red curve corresponds to $\hat{q} - q$ describing the production rate of oxygenated hydrocarbon. The green stoichiometric coefficient $z + q - \hat{z} - \hat{q}$ describes the rate of full oxidation reaction. Negative values of $\hat{q} - q$ (red curve) imply that the oxygen-containing hydrocarbon is converted back to hexadecane.

hydrocarbon. Sorption of oxygen in the hydrocarbons within the porous medium [8, 32, 47] can be either physical (physisorption) or chemical (chemisorption); physical adsorption is caused by physical forces, i.e., van der Waals interaction between adsorbent and the adsorbate. The adsorption process is exothermic. The physisorption energy is below 40 kJ/mol. The chemical adsorption is due to chemical reaction between the adsorbent and the adsorbate, which changes the structure of the adsorbent. The chemisorption energy is comparable to the energy of chemical bonds in reactions and it is 80 kJ/mol or even more [33]. The solubility of gas in a liquid decreases as temperature increases [8, 32, 47].

The temperature peaks in Fig. 7(left) indicate that an exothermic reaction zone is formed at temperatures above $330°C$, which moves along the reactor passing through TC-1 (red curve) at the top to TC-4 (green) at the bottom of the reactor. The exothermic reactions resulted in an average temperature increase of $100°C$. It is shown that the temperature increase is small and smooth at the top of the reactor (TC-1, TC-2), but less smooth at higher temperatures (TC-3, TC-4). A steep increase in temperature is an indication of a higher reaction rate at higher temperatures. The ultimate oil recovery for this experiment is 74%.

The viscosity and density of produced hydrocarbons are measured. These values turns out to be the same as the viscosity (2.9 cP) and density (761 kg/m^3) of hexadecane. This is intriguing evidence that the formation of oxygenated hydrocarbon may play a smaller role relative to oxygen dissolution in hydrocarbon than has been advocated in the literature.

Using the model reaction in Eq. (6.1), we can estimate the stoichiometric coefficient $\hat{q} - q$, which is proportional to the conversion rate of hexadecane to oxygen-containing hexadecane, see Fig. 7(right). Similarly, we estimate and plot in Fig. 7(right) the stoichiometric coefficient $z + q - \hat{z} - \hat{q}$, which describes the rate of complete scission of hydrocarbons. Initially, no hexadecane reacts with air. Then (after 100 min) oxygen starts to react with hexadecane. As shown in Fig. 7(right), part of the hexadecane is converted to oxygen-containing hexadecane, because no carbon oxides are produced. As temperature increases due to the external heater, more hexadecane is involved in chemical or physical adsorption of oxygen. After 300 min, a large part of oxygen-containing hexadecane is converted back to hexadecane, while the rest produces carbon oxides (note the increase of full oxidation rate, green curve in Fig. 7(right)). This agrees with the exothermic temperature history in Fig. 7(left).

In summary, in the low temperature range (below $250°C$), oxygen bonds physically or chemically in the low temperature oxidation zone with hydrocarbon. At a later stage, the oxygen-containing compound desorbs the oxygen or further undergoes oxidation reactions.

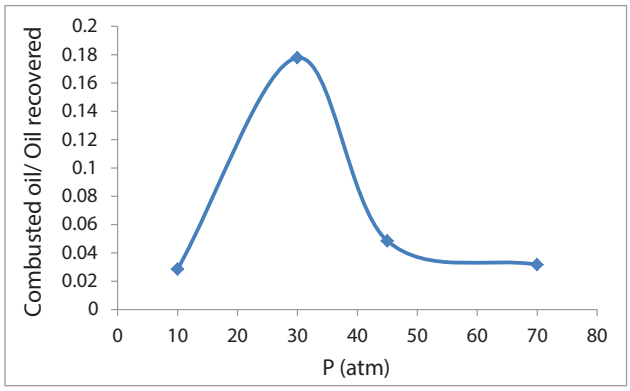

Figure 8: Ratio of burned to recovered hydrocarbon at the end of the experiments depending on pressure. The curve shows a spline approximation through the four experimental points.

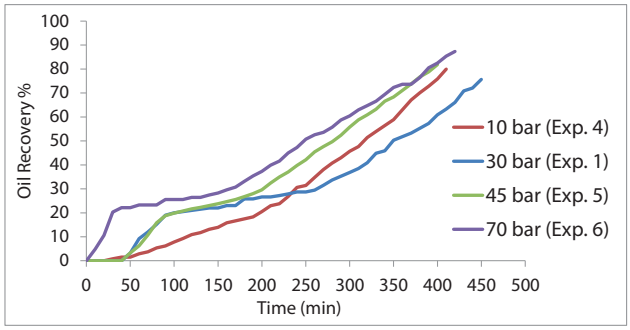

Figure 9: Oil recovery versus time under different pressures.

6.2 Efficiency of the air injection process

In the air injection process the amount of burned oil divided by the amount of recovered oil at the end of the experiment is shown in Fig. 8. The maximum ratio is attained at 30 bar (Exp. 1), while this ratio gets smaller both for lower (10 bar) and higher (45 and 70 bar) pressures. This trend agrees qualitatively with the analytical results on medium temperature oxidation process [44]. The recovered oil includes liquid and gaseous hydrocarbons. The mechanisms of liquid hydrocarbon recovery is flue gas displacement, (i.e., by nitrogen and combustion gases), while hydrocarbon recovery in gaseous phase is due to vaporization and distillation. The amount of burned oil varies in the range of $2-18\%$. As shown in Fig. 8, the maximum amount of oil is burned in the experiment at pressure of 30 bar.

Figure 9 shows the oil recovery versus time for four different pressures. We observe a rapid recovery increase at early times. This early production is caused mostly by depressurization and gas flood effects. MTO injection is more effective for oil recovery at higher pressures, as shown in Fig. 9, and confirmed theoretically in [44]. However, oil recovery at 30 bar appears to be lower than oil recovery at 10 bar, but this may be attributed to some problems in the experiment with the back pressure valve during initial part of the first experiment (Exp. 1). Note the striking qualitative agreement of Fig. 9 with the results of numerical simulations shown in Fig. 6. The three stages of the recovery process (cold gas displacement, ignition and MTO displacement) described in section 5.3 can be very well distinguished in the experimental curves of Fig. 9.

Conclusions

1. The applicability of air injection to volatile oil reservoirs at medium pressures and the MTO (medium temperature oxidation) efficiency have been studied experimentally in the laboratory and mathematically using simple 1-D models. The models consider vaporization, condensation and reaction with oxygen. The models indicate displacement efficiencies of almost $82 - 98\%$. Combustion leaves no residual oil, but a small part of the oil is burnt. The laboratory experiments indicate displacement efficiencies between $75 - 90\%$. The amount of oil burned in the air injection process relative to the amount of oil recovered in our laboratory experiments for hexadecane increased from 2% at 10 bar to 18% at 30 bar, and again decreased to 5% at 45 bar, after which it more or less remained constant. This trend was also predicted in previously obtained analytical results for the medium temperature oxidation process [44]. Finally, the MTO process is less efficient under higher air injection rates and the recovery is faster at higher pressures.

2. The following observations about the detailed combustion mechanisms in the presence of vaporization and condensation, based on a simple model with one volatile oil component and possibly a non-volatile component, can be made: vaporization occurs upstream of the combustion zone, a fact that is also confirmed by previously obtained analytical solutions [44]. The MTO method is effective when oil contains an appreciable amount of volatile oil, more than 20% in the example considered by us. The effect of the interaction between volatile and nonvolatile components at various concentrations, air injection rates and pressures is studied. The character of the MTO wave changes by altering the composition of the oil. Generally the solution consists of three types of waves, i.e., a thermal wave, an MTO wave and a saturation wave, all separated by constant state regions. The order between vaporization and oxidation in the MTO wave changes for different sets of conditions. For a predominantly light mixture, vaporization occurs upstream of the combustion process, a fact that confirms previously obtained analytical and numerical solutions for one component volatile oil [44, 35]. The combustion front velocity is high as less oil remains behind in the combustion zone. For oil with more non-volatile component (0.8 in volume fraction), the vaporization moves downstream of the combustion zone in the MTO wave. As more oil stays behind in the combustion zone, the velocity of the combustion zone is slower, albeit that the temperatures are much higher. Due to high temperatures, we conjecture a transition to the HTO process in this case, which would need to be confirmed by further research.

3. Numerical calculations establish a range of parameters for the bifurcation point between MTO and HTO in a two-component oil mixture. Indeed, the bifurcation point is mainly determined by the fraction of the non-volatile component. At the bifurcation the character of the combustion process changes from a vaporization-dominated to a combustion-dominated process.

4. A numerical model was formulated to simulate an injection of air into a one-dimensional porous medium filled with gas, water and light oil. The numerical solution consists of a thermal wave, a steam vaporization and condensation fronts, an MTO wave (oil reaction, vaporization and condensation), and three-phase saturation waves. It turns out that when the boiling point of the oil is near or slightly above the boiling point of water, the volatile oil condenses at the same location as the steam in the MTO wave, while steam vaporization occurs upstream. In this case the presence of water speeds up the oil recovery. The recovery curves (recovery fraction versus time) show striking universality properties, as they are almost independent of initial water saturation. However water condensation/vaporization effect is important, because the recovery curve is different (less efficient recovery), when water condensation is neglected in the model. If the boiling point of the oil is much higher than the

boiling point of water, the whole steam region moves ahead of the MTO wave. In this case, the presence of water has only a minor effect on the recovery efficiency, when initial water saturation is not high. However, the effect becomes negative, when the water saturation is high. Numerical simulations suggest that there is a bifurcation point (oil-boiling point) separating the case for which steam and oil condensation occur simultaneously in the MTO wave from the case where the steam region moves downstream of the combustion zone.

5. User-provided-equation based commercial software (COMSOL in our case) is able to solve combustion model equations of interest and can be applied to quantify the effect of diffusive processes, such as capillary diffusion, thermal conductivity and molecular diffusion. We used this software to obtain a numerical solution for comparison with an analytical solution in a zero diffusion model obtained previously, one/two-component oil models including volatile and non-volatile components, and a one-component oil model including water. We used this software to obtain a numerical solution for comparison with analytical solutions in zero diffusion models obtained previously. The qualitative behavior of the numerical solution is similar to the analytical solution in the absence of diffusive processes. The solution consists of three types of waves, i.e., a thermal wave, an MTO wave and saturation waves separated by constant state regions. The numerical model is capable of quantifying the effect of the diffusive processes, oil composition, pressure, injection rates and presence of water. The central scheme used in the finite element package, makes it possible to model situations both for low and high diffusion coefficients. The effect of the diffusive terms is as follows. Molecular diffusion lowers the temperature in the MTO region, but creates a small peak in the vaporization region. Capillary diffusion increases the temperature upstream of the MTO region. Higher capillary diffusion increases the recovery by gas displacement and lowers the recovery by combustion. The analytical solution, without diffusive terms, and the numerical solution become qualitatively different at very high capillary diffusion coefficients. The effect of thermal diffusion smoothes the thermal wave and widens the hydrocarbon vapor peak.

6. Experiments can validate various aspects of the developed models: A set of experiments have been designed that enables investigation of the medium pressure air injection process at low injection rate in consolidated porous media saturated with oil [44, 34]. The experiments used hexadecane. Our laboratory experiments indicate recoveries between $75-90\%$. Sufficient fuel is available to consume the injected oxygen, and only 0.5% of oxygen was found in the produced gas. The experiments show evidence that the reaction [11] occur in two stages. In the first stage, oxygen adsorption takes place at low temperatures before the bond-scission combustion reactions occur. The sorbed oxygen bonds with hydrocarbon physically or chemically leading to complete uptake of oxygen from the injected air stream at low temperatures. Then the oxygen-containing compound releases the oxygen at higher temperatures and partially reconverts to hexadecane, which is later produced, and partially undergoes a combustion reaction releasing carbon oxides and possibly also water. The produced liquid is hexadecane; it is not altered by the oxidation reaction because it has the same viscosity and density. It is recalled that oxygenated hydrocarbons have higher viscosities [45]. The experimental results also confirmed the three stages of the recovery process, which are characterized by almost constant recovery rates, as discovered in numerical simulations. These stages correspond to the cold gas displacement, ignition stage and MTO displacement recovery.

Acknowledgments

This research was carried out within the context of the first round of the ISAPP Knowledge Centre. This round of ISAPP (Integrated Systems Approach to Petroleum Production) is a joint

project of the Netherlands Organization of Applied Scientific Research TNO, Shell International Exploration and Production, and Delft University of Technology. In addition, this paper was also supported by grants of PRH32(ANP 731948/2010, PETROBRAS 6000.0061847.10.4), FAPERJ(E-26/102.965/2011, E-26/111.416/2010, E-26/110.658/2012, E-26/110.237/2012, E-26/111.369/2012) and CNPq (301564/2009-4,472923/2010-2, 477907/2011-3, 305519/2012-3, 402299/2012-4, 470635/2012-6),FAPERJ E-26/110.114/2013 and CAPES/Nuffic 024/2011.The authors thank TU Delft and IMPA for providing the opportunity for this work.

References

[1] J. H. Abou-Kassem, S. M. Farouq Ali, and J. Ferrer. Appraisal of steamflood models. *Rev. Tec. Ing.*, 9:45–58, 1986.

[2] L. Adetunji and R. Teigland. Light-oil air-injection performance: sensitivity to critical parameters. In *SPE Annual Technical Conference and Exhibition*, volume SPE-96844, 2005.

[3] S. Akin, M.V. Kok, S. Bagci, and O. Karacan. Oxidation of heavy oil and their SARA fractions: its role in modeling in-situ combustion. SPE 63230, 2000.

[4] A. V. Azevedo, A. J. deSouza, D. Marchesin, and B. Plohr. The solution by the wave curve method of three-phase flow in virgin reservoirs. *Transport in Porous Media*, 83(1):99–125, 2010.

[5] Tayfun Babadagli. Mature field development-a review. In *SPE Europec/EAGE Annual Conference*. Society of Petroleum Engineers, 2005.

[6] C.H. Bamford and C.E.H. Tipper. *Comprehensive Chemical Kinetics, Vol. 17, Gas-phase Combustion*. Elsevier, 1977.

[7] Y. Barzin, R. Moore, S. Mehta, M. Ursenbach, and F. Tabasinejad. Impact of Distillation on the Combustion Kinetics of high pressure air injection (HPAI). In *SPE 129691-Improved Oil Recovery Symposium*, 2010.

[8] Rubin Battino, Timothy R Rettich, and Toshihiro Tominaga. The solubility of oxygen and ozone in liquids. *Journal of physical and chemical reference data*, 12(2):163–178, 1983.

[9] A. Bayliss and B.J. Matkowsky. From traveling waves to chaos in combustion. *SIAM J. Appl. Math.*, 54:147–174, 1994.

[10] Martin Blunt, F John Fayers, and Franklin M Orr Jr. Carbon dioxide in enhanced oil recovery. *Energy Conversion and Management*, 34(9):1197–1204, 1993.

[11] J. Bruining, A.A. Mailybaev, and D. Marchesin. Filtration combustion in wet porous medium. *SIAM J. Appl. Math.*, 70:1157–1177, 2009.

[12] J Bruining and D Marchesin. Maximal oil recovery by simultaneous condensation of alkane and steam. *Physical Review E*, 75(3):036312, 2007.

[13] L.M. Castanier and W.E. Brigham. Modifying in-situ combustion with metallic additives. *In Situ*, 21(1):27–45, 1997.

[14] L.M. Castanier and W.E. Brigham. Upgrading of crude oil via in situ combustion. *Journal of Petroleum Science and Engineering*, 39:125–136, 2003.

[15] C. Clara, M. Durandeau, G. Quenault, and T.H. Nguyen. Laboratory studies for light-oil air injection projects: potential application in handil field. *SPE Reservoir Evaluation & Engineering*, 3(3):239–248, 2000.

[16] M. Fassihi, W. Brigham, and H. Ramey Jr. Reaction kinetics of in-situ combustion: Part 1-observations. *Old SPE Journal*, 24(4):399–407, 1984.

[17] M.R. Fassihi, D.V. Yannimaras, and V.K. Kumar. Estimation of recovery factor in light-oil air-injection projects. *SPE Reservoir Engineering*, 12:173–178, 1997.

[18] M.R. Fassihi, D.V. Yannimaras, E.E. Westfall, and T.H. Gillham. Economics of light oil air injection projects. In *SPE/DOE Improved Oil Recovery Symposium*, 1996.

[19] W. Fickett and W.C. Davis. *Detonation: Theory and Experiment*. Dover, Mineola, N.Y., 2011.

[20] E.M. Fisher, W.J. Pitz, H.J. Curran, and C.K. Westbrook. Detailed chemical kinetic mechanisms for combustion of oxygenated fuels. *Proceedings of the Combustion Institute*, 28(2):1579–1586, 2000.

[21] N.P. Freitag and B. Verkoczy. Low-temperature oxidation of oils in terms of SARA fractions: why simple reaction models don't work. *Journal of Canadian Petroleum Technology*, 44(3):54–61, 2005.

[22] P. Germain and J.L. Geyelin. Air injection into a light oil reservoir: the Horse Creek project. In *Middle East Oil Show and Conference, Bahrain*, 15-18 March 1997.

[23] M. Gerritsen, A. Kovscek, L. Castanier, J. Nilsson, R. Younis, and B. He. Experimental investigation and high resolution simulator of in-situ combustion processes; 1. simulator design and improved combustion with metallic additives. In *SPE International Thermal Operations and Heavy Oil Symposium and Western Regional Meeting*, 2004.

[24] T.H. Gillham, B.W. Cerveny, M.A. Fornea, and D. Bassiouni. Low cost IOR: an update on the W. Hackberry air injection project. In *Paper SPE-39642 presented at the SPE/DOE Improved Oil Recovery Symposium, Tulsa, Oklahoma, April, 19–22*, 1998.

[25] T.H. Gillham, B.W. Cerveny, E.A. Turek, and D.V. Yannimaras. Keys to increasing production via air injection in Gulf Coast light oil reservoirs. In *SPE Annual Technical Conference and Exhibition, SPE 38848-MS*, 1997.

[26] M. Greaves, S. Ren, R. Rathbone, T. Fishlock, and R. Ireland. Improved residual light oil recovery by air injection (LTO process). *Journal of Canadian Petroleum Technology*, 39(1), 2000.

[27] M. Greaves, T.J. Young, S. El-Usta, R.R. Rathbone, S.R. Ren, and T.X. Xia. Air injection into light and medium heavy oil reservoirs: combustion tube studies on west of Shetlands Clair oil and light Australian oil. *Chemical Engineering Research and Design*, 78(5):721–730, 2000.

[28] D. Gutierrez, F. Skoreyko, R. Moore, S. Mehta, and M. Ursenbach. The challenge of predicting field performance of air injection projects based on laboratory and numerical modelling. *Journal of Canadian Petroleum Technology*, 48(4):23–33, 2009.

[29] D. Gutierrez, A. Taylor, V. Kumar, M. Ursenbach, R. Moore, and S. Mehta. Recovery factors in high-pressure air injection projects revisited. *SPE Reservoir Evaluation & Engineering*, 11(6):1097–1106, 2008.

[30] W.C. Hardy, P.B. Fletcher, J.C. Shepard, E.W. Dittman, and D.W. Zadow. In-situ combustion in a thin reservoir containing high-gravity oil. *J. of Petroleum Technology*, 24(2):199–208, 1972.

[31] F.G. Helfferich. *Kinetics of Multistep Reactions*. Elsevier, 2004.

[32] Lu-Kwang Ju and Chester S Ho. Oxygen diffusion coefficient and solubility in n-hexadecane. *Biotechnology and bioengineering*, 34(9):1221–1224, 1989.

[33] J.U. Keller and R. Staudt. *Gas Adsorption Equilibria: Experimental Methods and Adsorptive Isotherms*. Springer, 2005.

[34] N. Khoshnevis Gargar, A.A. Mailybaev, J. Bruining, and D. Marchesin. Compositional effects in light oil recovery by air injection: Vaporization vs. combustion. *Accepted in Journal of Porous Media*, 2013.

[35] N. Khoshnevis Gargar, A.A. Mailybaev, J. Bruining, and D. Marchesin. Diffusive effects on recovery of light oil by medium temperature oxidation. *Accepted in Transport in Porous Media*, 2013.

[36] M.V. Kok and C.O. Karacan. Behavior and effect of SARA fractions of oil during combustion. *SPE Reservoir Evaluation and Engineering*, 3:380–385, 2000.

[37] A.G. Kulikovskii and N.T. Pashchenko. Propagation regimes of self-supported light-detonation waves. *Fluid Dynamics*, 40(5):818–828, 2005.

[38] O. Levenspiel. *Chemical reaction engineering*. John Wiley & Sons, 1999.

[39] C.Y. Lin, W.H. Chen, and W.E. Culham. New kinetic models for thermal cracking of crude oils in in-situ combustion processes. *SPE Reservoir Engineering*, 2:54–66, 1987.

[40] C.Y. Lin, W.H. Chen, S.T. Lee, and W.E. Culham. Numerical simulation of combustion tube experiments and the associated kinetics of in-situ combustion processes. *SPE Journal*, 24:657–666, 1984.

[41] A.A. Mailybaev, J. Bruining, and D. Marchesin. Analysis of in situ combustion of oil with pyrolysis and vaporization. *Combustion and Flame*, 158(6):1097–1108, 2011.

[42] A.A Mailybaev, J. Bruining, and D. Marchesin. Analytical formulas for in-situ combustion. *SPE Journal*, 16(03):513–523, 2011.

[43] A.A. Mailybaev, D. Marchesin, and J. Bruining. Resonance in low-temperature oxidation waves for porous media. *SIAM Journal on Mathematical Analysis*, 43:2230, 2011.

[44] A.A. Mailybaev, D. Marchesin, and J. Bruining. Recovery of light oil by medium temperature oxidation. *Transport in Porous Media*, 97(3):317–343, 2013.

[45] DD Mamora. New findings in low-temperature oxidation of crude oil. In *SPE Asia Pacific Oil and Gas Conference*, 1995.

[46] D. Marchesin and B.J. Plohr. Wave structure in WAG recovery. SPEJ. 6 (2): 209-219. Technical report, SPE-71314-PA, 2001.

[47] EC Markham and Arthur F Benton. The adsorption of gas mixtures by silica. *Journal of the American Chemical Society*, 53(2):497–507, 1931.

[48] B.J. Matkowsky and G. Sivashinsky. Propagation of a pulsating reaction front in solid fuel combustion. *SIAM J. Appl. Math.*, 35:465–478, 1978.

[49] S.R. Ren, M. Greaves, and R.R. Rathbone. Air injection LTO process: an IOR technique for light-oil reservoirs. *SPE Journal*, 7(1):90–99, 2002.

[50] G.L. Schott. Kinetic studies of hydroxyl radicals in shock waves. iii. the OH concentration maximum in the hydrogen-oxygen reaction. *The Journal of Chemical Physics*, 32:710, 1960.

[51] D.A. Schult, B.J. Matkowsky, V.A. Volpert, and A.C. Fernandez-Pello. Forced forward smolder combustion. *Combustion and Flame*, 104:1–26, 1996.

[52] W. Schulte. Challenges and strategy for increased oil recovery. In *International Petroleum Technology Conference*, 2005.

[53] G.J. Sharpe and S. Falle. One-dimensional nonlinear stability of pathological detonations. *Journal of Fluid Mechanics*, 414(1):339–366, 2000.

[54] A.T. Turta and A.K. Singhal. Reservoir engineering aspects of light-oil recovery by air injection. *SPE Reservoir Evaluation & Engineering*, 4(4):336–344, 2001.

[55] JR Waggoner, JL Castillo, Larry W Lake, et al. Simulation of EOR processes in stochastically generated permeable media. *SPE formation evaluation*, 7(02):173–180, 1992.

[56] C.W. Wahle, B.J. Matkowsky, and A.P. Aldushin. Effects of gas-solid nonequilibrium in filtration combustion. *Combust. Sci. and Tech.*, 175:1389–1499, 2003.

[57] H.J. Welge. A simplified method for computing oil recovery by gas or water drive. *Transactions of AIME*, 195:91–98, 1952.

[58] W.W. Wood and Z.W. Salsburg. Analysis of steady-state supported one-dimensional detonations and shocks. *Physics of Fluids*, 3:549–566, 1960.

[59] Z. Xu, L. Jianyi, S. Liangtian, L. Shilun, and L. Weihua. Research on the mechanisms of enhancing recovery of light-oil reservoir by air-injected low-temperature oxidation technique. *Natural Gas Industry*, 24:78–80, 2004.